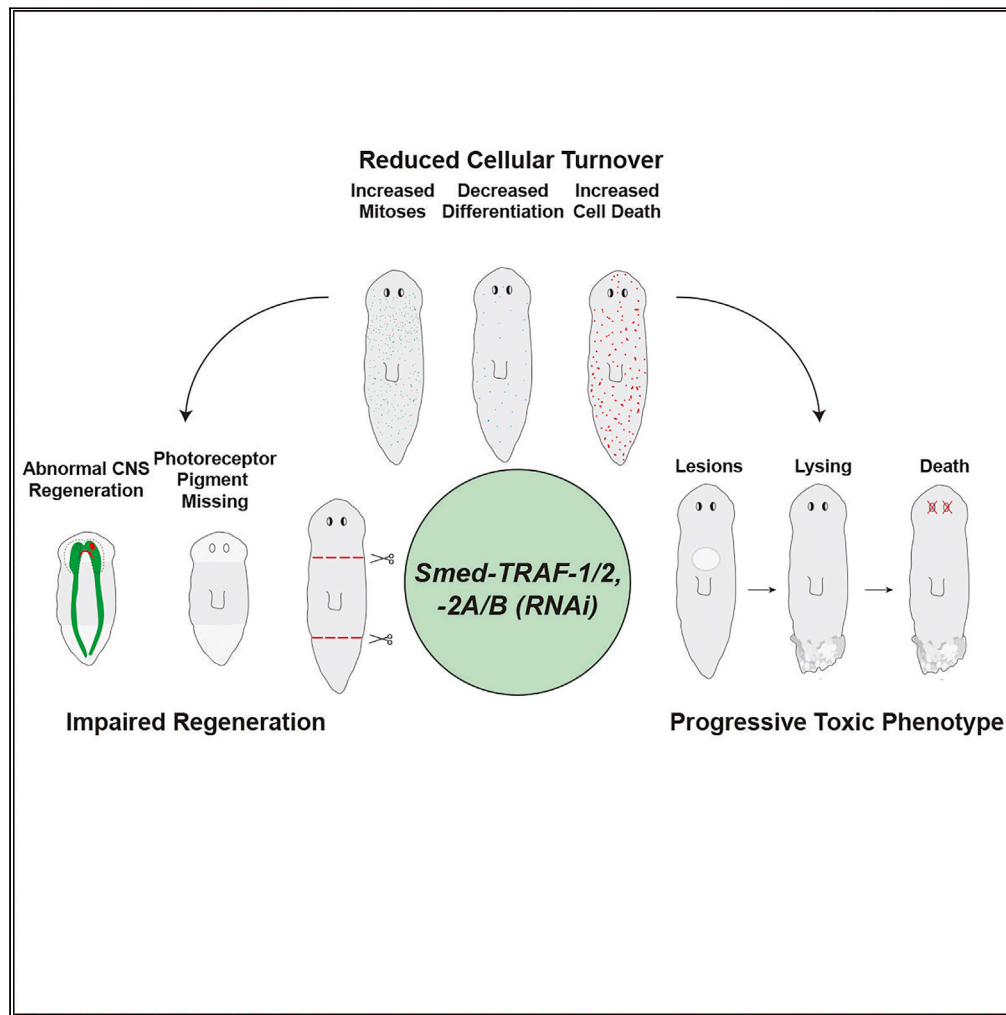


Article

TRAF-like Proteins Regulate Cellular Survival in the Planarian *Schmidtea mediterranea*



Benjamin Ziman,
Paul G.
Barghouth, Eli
Isael Maciel,
Néstor J. Oviedo

noviedo2@ucmerced.edu

HIGHLIGHTS

The expression of *Smed-TRAF-1/2, -2A/B* is enriched in the digestive system

Planarian TRAF-like proteins regulate the systemic cellular turnover

Loss of *Smed-TRAF-1/2, -2A/B* leads to impaired tissue regeneration



Article

TRAF-like Proteins Regulate Cellular Survival in the Planarian *Schmidtea mediterranea*Benjamin Ziman,^{1,2,4} Paul G. Barghouth,^{1,2,4} Eli Isael Maciel,^{1,2,4} and Néstor J. Oviedo^{1,2,3,5,*}

SUMMARY

Tissue homeostasis relies on the timely renewal of cells that have been damaged or have surpassed their biological age. Nonetheless, the underlying molecular mechanism coordinating tissue renewal is unknown. The planarian *Schmidtea mediterranea* harbors a large population of stem cells that continuously divide to support the restoration of tissues throughout the body. Here, we identify that TNF Receptor Associated Factors (TRAFs) play critical roles in cellular survival during tissue repair in *S. mediterranea*. Disruption with RNA-interference of TRAF signaling results in rapid morphological defects and lethality within 2 weeks. The TRAF phenotype is accompanied by an increased number of mitoses and cell death. Our results also reveal TRAF signaling is required for proper regeneration of the nervous system. Taken together, we find functional conservation of TRAF-like proteins in *S. mediterranea* as they act as crucial regulators of cellular survival during tissue homeostasis and regeneration.

INTRODUCTION

TNF receptor associated factors (TRAFs) are a family of adaptor proteins that associate with the tumor necrosis factor superfamily, pattern recognition receptors, and other cytokine receptors (Arch et al., 1998; Park, 2018; Xie, 2013). TRAF proteins aid in linking upstream receptors to downstream effects, including transcription factors such as NF- κ B, AP-1, and IRFs, which are key players in cell proliferation, survival, death, and immune system functions (Honda and Taniguchi, 2006; Karin et al., 1997; Piva et al., 2006). Since the 1990s, there has been an identification of seven mammalian TRAFs proteins, characterized by the presence of the TRAF domain (Park, 2018). The TRAF domains contain both a TRAF-N (coiled-coiled) domain and a TRAF-C (meprin and TRAF-C homology "MATH") domain at the C terminus, which binds to intracellular signaling molecules and receptors, respectively (Park, 2018). However, TRAF1 lacks the RING domain at the N terminus and, therefore, does not possess ligase function (Deshaies and Joazeiro, 2009; Yang and Sun, 2015). Additionally, TRAF7 lacks the entire TRAF homology domain, making it controversial if it is considered a true TRAF family protein (Arkee and Bishop, 2019; Bishop et al., 2019). Loss of TRAF proteins can lead to increased inflammation and early lethality (e.g., TRAF 2,3,6), making it challenging to understand their roles in adult tissue homeostasis (Chiffolleau et al., 2003; Lomaga et al., 1999; Xu et al., 1996; Yeh et al., 1997).

The planarian flatworm *Schmidtea mediterranea* is an attractive alternative model system to study the functionality of embryonically lethal genes in the adult body (Peiris et al., 2012; Thiruvalluvan et al., 2018; Ziman et al., 2020). *S. mediterranea* is a classical model for studying tissue regeneration and stem cell regulation during organismal, cellular turnover, due to an abundant population of pluripotent stem cells known as neoblasts (Elliott and Sánchez Alvarado, 2013; Reddien and Alvarado, 2004). Several reports have suggested the presence of TRAF proteins in *S. mediterranea* (Rouhana et al., 2010; Tu et al., 2015; Forsthoefel et al., 2019; Arnold et al., 2016; Peiris et al., 2014; Wurtzel et al., 2015; Wenemoser et al., 2012; Swapna et al., 2018; Pang et al., 2016; Maciel et al., 2019; Tsoumtsas et al., 2017; Sandmann et al., 2011; Grohme et al., 2018; Ross et al., 2018; Hu et al., 2019). Most of these studies used the presence of MATH domains (make up the functional C-terminal domains) as the main feature to catalog TRAF proteins in planarians. However, the MATH domain is not specific to TRAF proteins and has been found in various other proteins, which can be misleading to call these true TRAF genes in the planarian model (Zapata et al., 2001). Since none of the putative TRAF proteins identified in planarians have been functionally characterized, we performed more exhaustive phylogenetic and functional studies to gain insights about the role of the TRAF proteins during cellular turnover and regeneration.

¹Department of Molecular and Cell Biology, University of California, Merced, CA 95343, USA

²Quantitative and Systems Biology Graduate Program, University of California, Merced, CA 95343, USA

³Health Sciences Research Institute, University of California, Merced, CA 95343, USA

⁴These authors contributed equally

⁵Lead Contact

*Correspondence: noviedo2@ucmerced.edu
<https://doi.org/10.1016/j.isci.2020.101665>



We identified two putative TRAF-like proteins (*Smed-TRAF-1/2*, and *-2A/B*) in the planarian *S. mediterranea*, which possess molecular similarities with their human counterparts. Loss of *Smed-TRAF-1/2* or *Smed-TRAF-2A/B* led to morphological defects, including lesions and lysing. Furthermore, knockdown of *Smed-TRAF-1/2* had more noticeable defects in the anterior region, whereas knockdown of *Smed-TRAF-2A/B* was more prominent in the posterior portion of intact animals. Loss of *Smed-TRAF-1/2* or *Smed-TRAF-2A/B* led to increased cell death, accompanied by hyper-proliferation and impaired differentiation. The progression of the phenotype ultimately led to 100% of animals dying within 15 days of RNAi. Additionally, we found that, upon amputation, *Smed-TRAF-1/2(RNAi)* and *Smed-TRAF-2A/B(RNAi)* animals had impaired regeneration, leading to disrupted central nervous system (CNS) formation. Overall, we found *Smed-TRAF-1/2* and *Smed-TRAF-2A/B* to be essential regulators of cell survival and tissue regeneration.

RESULTS

Identification of TRAF-like Proteins in *S. mediterranea*

Previous reports (*in silico* and *in vivo*) using planarian as a model system have shown elevated TRAF expression during tissue homeostasis and regeneration (Rouhana et al., 2010; Sandmann et al., 2011; Wenemoser et al., 2012; Wurtzel et al., 2015). However, owing to the abundant amount of TRAF/MATH homology domains found within the *S. mediterranea* genome (i.e., higher than 121 transcripts) analysis of TRAF functions has been somewhat inconclusive (Forsthoefel et al., 2019; Swapna et al., 2018). Thus, we began by assessing the amount of TRAF homologs found within the recently published PlanMine3.0 database (Rozanski et al., 2019). Using the PlanNET database, we isolated planarian transcripts according to PfamID (e.g., MATH/TRAF PF00917) (Castillo-Lara and Abril, 2018). This analysis yielded a more significant number of contigs with human homology relative to the Toronto database (e.g., 282 versus 121 transcripts) (Figure S1A) (Swapna et al., 2018). To begin the filtration process, we BLASTed each of the six individual human TRAF genes into PlanMine3.0 using an e-value cutoff of 1.0×10^{-5} , and this produced approximately 150–212 contigs per TRAF homolog (Figure S1B). Furthermore, we used a more stringent cutoff of 1.0×10^{-30} , thus reducing the contig output to 1–13 per homolog. A majority of the transcripts per human homolog were redundant among each other, and analysis of their conserved domains yielded partial or lacking signature TRAF domains (e.g., Ring and zinc fingers). We identified two unique and top-ranking putative proteins for TRAF-1 and TRAF-2 with conserved signature domains and high percent identities (i.e., 42% and 31%, respectively). TRAF1 is distinctively recognized by a single and highly conserved MATH domain (Zapata et al., 2007). We found this is consistent for the putative TRAF-1 protein in *S. mediterranea*, whereas the putative TRAF-2 protein additionally includes the signature ring and zinc finger domains. Phylogenetic analysis suggested these TRAF-like proteins in the planarian *S. mediterranea* are likely an out-group from vertebrate TRAF proteins in a similar fashion to *Drosophila melanogaster*. These findings were consistent with previously identified planarian TRAF proteins (Rouhana et al., 2010; Wurtzel et al., 2015). The putative TRAF-1 protein in planarian is likely a co-ortholog of the vertebrate TRAF-1 and TRAF-2 proteins; therefore, we decided to name it *Smed-TRAF-1/2*. Our findings also suggest the putative TRAF-2 in *S. mediterranea* is distant from the vertebrate TRAF-2; however, it appeared to be a co-ortholog to *D. japonica* TRAF-2A and TRAF-2B, which led to the naming convention *Smed-TRAF-2A/B* (Figure S2). Altogether, our analysis identified two planarian TRAF-like proteins; however, further analysis of the 121 MATH_TRAF transcripts will be required to determine with certainty the total amount of TRAF's in the *S. mediterranea* genome.

TRAF-like Proteins *Smed-TRAF-1/2* and *Smed-TRAF-2A/B* Are Required for Homeostatic Function

Our results using whole-mount *in situ* hybridization revealed the expression of *Smed-TRAF-1/2* and *-2A/B* is ubiquitous and enriched in the planarian intestine (Figure 1A), which is consistent with previous findings (Forsthoefel et al., 2019; Tu et al., 2015; Wenemoser et al., 2012; Wurtzel et al., 2015). Additionally, we found the expression of *Smed-TRAF-1/2* and *Smed-TRAF-2A/B* appears to increase upon exposure to ionizing radiation (Figure S3A), similar to previous observations (Rouhana et al., 2010; Wenemoser et al., 2012). Consistently, both *Smed-TRAF-1/2* and *Smed-TRAF-2A/B* were predicted to be highly expressed across neoblasts and postmitotic cells (Figure S3B). Our findings suggest *Smed-TRAF-1/2* and *-2A/B* are broadly expressed across the planarian body involving neoblasts and postmitotic cells.

Functional studies were performed to knock down gene expression for individual TRAF-like proteins using RNA interference (RNAi) (Figure 1B). We found that animals subjected to *Smed-TRAF-1/2(RNAi)*

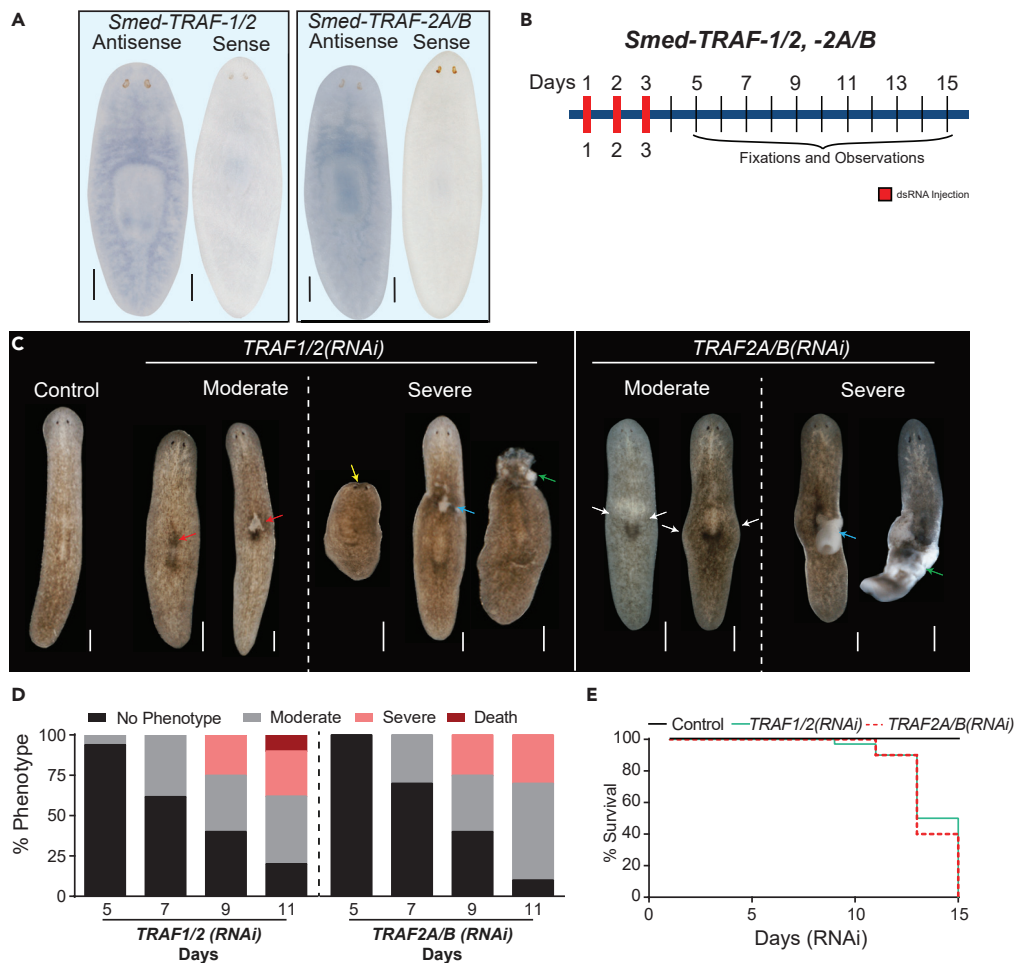


Figure 1. *Smed-TRAF-1/2* and *Smed-TRAF-2A/B* Are Vital Homeostatic Regulators

(A) Whole-mount *in situ* hybridization using both sense and antisense probes against *Smed-TRAF-1/2* and *Smed-TRAF-2A/B*. Gene expression was found to be enriched in the GI tract. Scale bars 200 μ m.

(B) RNAi schedule for Both *Smed-TRAF-1/2* and *Smed-TRAF-2A/B* based on micro-injections with dsRNA. Red bars represent injections. Fixations and observations occurred between 5 and 15 days after the first injection.

(C) Representative images displaying observed morphological defects in *Smed-TRAF-1/2(RNAi)* and *Smed-TRAF-2A/B(RNAi)* animals. Phenotypes were categorized as being either moderate (left) or severe (right) based on physical manifestations. Moderate phenotypes consisted of bloating (white arrows) or small lesions (red arrow) around the pharynx area. In contrast, Severe phenotypes were characterized by reduction of anterior tissue (yellow arrow), more pronounced lesions (blue arrows), or lysing (green arrows). Scale bars, 200 μ m.

(D) Graphical representation of the percent of animals displaying phenotypes through the progression of the RNAi time course. The onset of the moderate phenotypes began between 5 and 7 days after the first injection, whereas severe phenotypes started appearing after 9 days after the first injection.

(E) Survival plot of both *Smed-TRAF-1/2(RNAi)* (solid green) and *Smed-TRAF-2A/B(RNAi)* (dashed red) animals. RNAi of both *Smed-TRAF-1/2* and *Smed-TRAF-2A/B* was extremely toxic, leading to 100% of the animals dying within 15 days after the first injection.

and *Smed-TRAF-2A/B(RNAi)* developed morphological defects that were evident within the first week post-RNAi and worsened over time. The (moderate) phenotype first appeared approximately 5–7 days after the first injection, leading to small lesions or bloating near the pharynx in *Smed-TRAF-1/2(RNAi)* and *Smed-TRAF-2A/B(RNAi)* animals, respectively (Figures 1C and 1D). This was also accompanied by impaired movement, which was prominent in *Smed-TRAF-2A/B(RNAi)* animals. The onset of the more aggressive phenotype (severe) started occurring around 9 days after the first injection (Figures 1C and 1D). The severe phenotype was characterized by head regression and anterior lesion in *Smed-TRAF-1/2(RNAi)* animals and lesion near the pharynx or in the posterior of *Smed-TRAF-2A/B(RNAi)* animals (Figures 1C and 1D). The

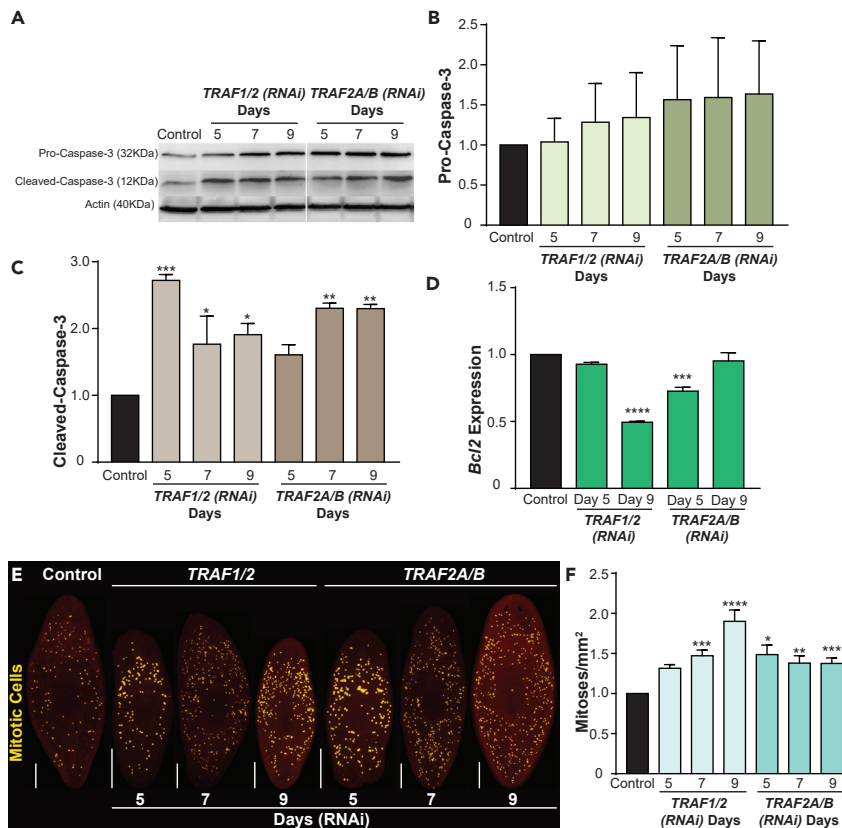


Figure 2. *Smed-TRAF-1/2* and *Smed-TRAF-2A/B* Are Important Regulators of Cell Survival

(A–C) Western blots and subsequent quantification (fold change) for both Pro-Caspase-3 and Cleaved Caspase-3 in *Smed-TRAF-1/2(RNAi)* and *Smed-TRAF-2A/B(RNAi)* animals. Actin was used as an internal control. A single lane from the blot was removed, as indicated by the gap in the image. Protein was extracted from more than 30 animals with at least two technical replicates. * $p < 0.05$; ** $p < 0.01$; *** $p < 0.001$; one-way ANOVA.

(D) Gene expression levels of pro-survival marker *Bcl2* in both *Smed-TRAF-1/2(RNAi)* and *Smed-TRAF-2A/B(RNAi)* animals. Data were obtained from triplicates. *** $p < 0.001$; **** $p < 0.0001$; one-way ANOVA.

(E) Whole-mount immunohistochemistry using the mitotic marker Anti-Phospho-histone H3 (serine-10) (H3P) antibody in *Smed-TRAF-1/2(RNAi)* and *Smed-TRAF-2A/B(RNAi)* animals. Scale bars, 200 μm .

(F) The number of mitotic events in *Smed-TRAF-1/2(RNAi)* and *Smed-TRAF-2A/B(RNAi)* animals, represented as fold change. Data were obtained using at least five animals with at least one technical replicate. * $p < 0.05$; ** $p < 0.01$; *** $p < 0.001$; **** $p < 0.0001$; one-way ANOVA. Data are represented as mean \pm SEM.

progression of these phenotypes led to lysing and animals dying within 2 weeks post-RNAi (Figure 1E). Overall, we found that RNAi of *Smed-TRAF-1/2* and *Smed-TRAF-2A/B* led to morphological abnormalities, suggesting that these TRAF-like proteins may regulate critical homeostatic functions.

TRAF-like Proteins *Smed-TRAF-1/2* and *Smed-TRAF-2A/B* Are Required for Cell Survival

TRAF proteins are known to play critical roles in cell survival (Piva et al., 2006; Karin et al., 1997). To understand how the TRAF phenotype progressed from moderate (i.e., small morphological defect) to severe (i.e., lesions and lysing), we quantified cell death using the apoptotic marker Caspase-3 (Figure 2A). Pro-Caspase-3 becomes cleaved and involved in the execution of cellular apoptosis (Nicholson and Thornberry, 1997). We found that Pro-Caspase-3 was increased after the fifth day of RNAi in both *Smed-TRAF-1/2(RNAi)* and *Smed-TRAF-2A/B(RNAi)* animals (Figure 2B). Cleaved Caspase-3 peaked at 5 days and remained increased (~2-fold) during the first 9 days after the first injection in *Smed-TRAF-1/2(RNAi)* animals. In contrast, *Smed-TRAF-2A/B(RNAi)* led to increases in Cleaved Caspase-3 that were more prominent and sustained after day 7 post-RNAi (Figure 2C). These changes were accompanied by a reduction in gene expression for pro-survival factor *Smed-Bcl2* in *Smed-TRAF-1/2(RNAi)* and *Smed-TRAF-2A/B(RNAi)* animals 9 days and 5 days after the first RNAi injection, respectively (Figure 2D). Since the phenotypes

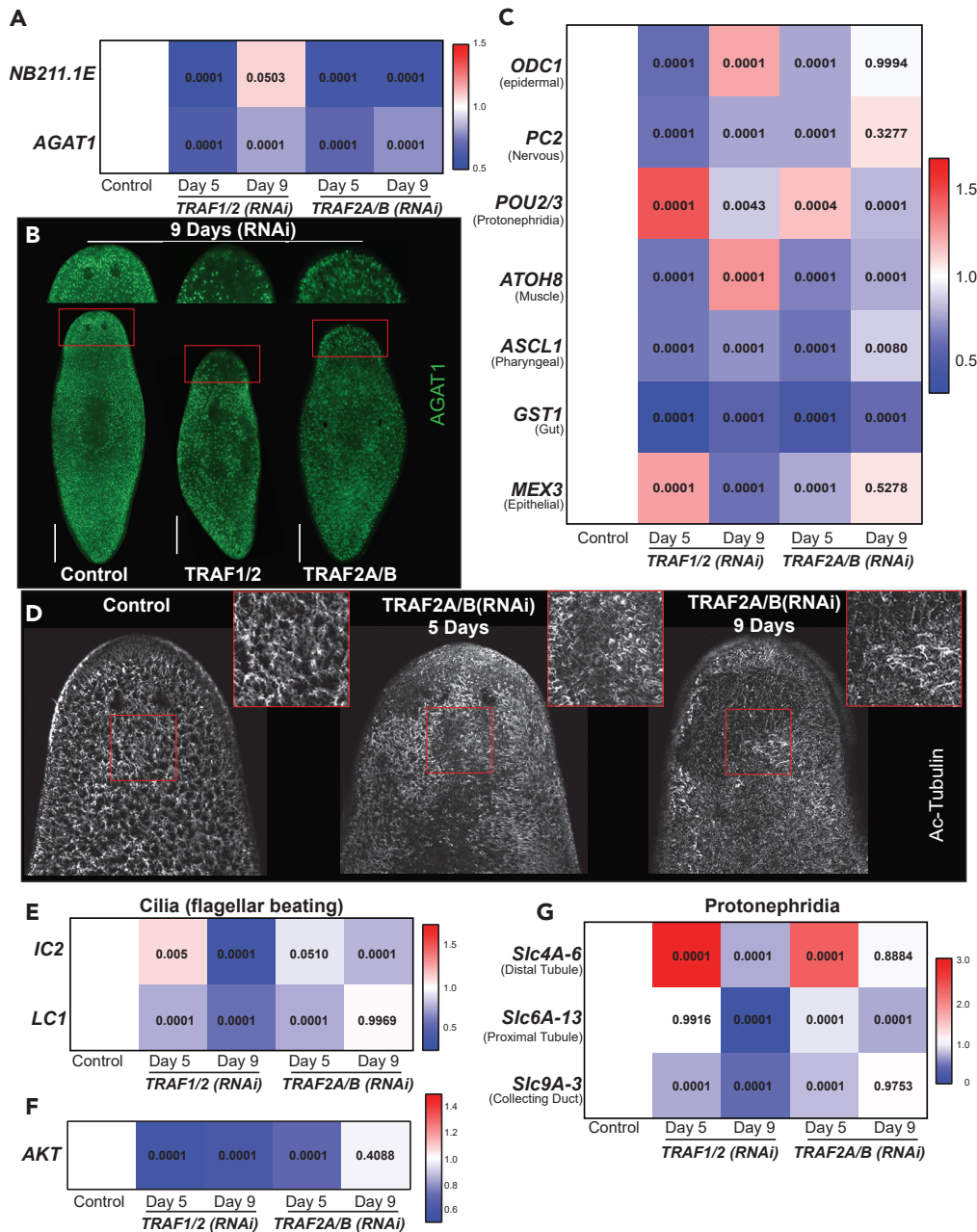


Figure 3. Loss of *Smed-TRAF-1/2* and *Smed-TRAF-2A/B* Reduces Differentiation Marker Gene Expression and Cilia Distribution, Possibly through the Regulation of AKT

(A) Heatmap representing gene expression for early (*nb211.1E* or *Smed-prog-1*) and late (*Smed-agat-1*) neoblast progeny markers in *Smed-TRAF-1/2(RNAi)* and *Smed-TRAF-2A/B(RNAi)* animals.

(B) Whole-mount fluorescent *in situ* hybridization for *Smed-agat-1* gene expression in *Smed-TRAF-1/2(RNAi)* and *Smed-TRAF-2A/B(RNAi)* animals. Images are from intact animals, displaying no morphological abnormalities, and representative of the group. Scale bars, 200 μ m.

(C) Heatmap representing gene expression levels of differentiation markers of various cell types in *Smed-TRAF-1/2(RNAi)* and *Smed-TRAF-2A/B(RNAi)* animals.

(D) Whole-mount immunohistochemistry using the cilia marker Anti- α -Ac-tubulin antibody in control and *Smed-TRAF-2A/B(RNAi)* animals. Images are representative of each group. Insets depict the distribution of cilia.

(E) Heatmap representing gene expression levels for markers of flagellar beating cilia, *IC2*, and *LC1* in *Smed-TRAF-1/2(RNAi)* and *Smed-TRAF-2A/B(RNAi)* animals.

(F) Heatmap representing gene expression levels of *AKT* in *Smed-TRAF-1/2(RNAi)* and *Smed-TRAF-2A/B(RNAi)* animals.

Figure 3. Continued

(G) Heatmap representing gene expression levels for markers of protonephridia (*Slc4a-6*- distal tubules, *Slc6a-13*- proximal tubules, *Slc9a-3*- collecting ducts) in *Smed-TRAF-1/2(RNAi)* and *Smed-TRAF-2A/B(RNAi)* animals. The reference scale bar for gene expression denotes high expression in red and low expression in blue. Statistical p values (one-way ANOVA) displayed within each cell. Data were obtained from triplicates.

of *Smed-TRAF-1/2; -2A/B(RNAi)* led to increases in cell death and tissue damage, we evaluated whether cell division was also altered under these circumstances. The results revealed that both *Smed-TRAF-1/2(RNAi)* and *Smed-TRAF-2A/B(RNAi)* animals displayed increased mitotic events beginning 5 days after the first dsRNA injection. The dividing cells peaked as the phenotype progressed in *Smed-TRAF-1/2(RNAi)* animals, whereas they remained uniformly elevated throughout the 9 days in *Smed-TRAF-2A/B(RNAi)* animals (Figures 2E and 2F). Overall, this suggests that *Smed-TRAF-1/2* and *Smed-TRAF-2A/B* regulate cell survival and proliferation in *S. mediterranea*.

Although there was an increase in cell division after *Smed-TRAF-1/2(RNAi)* and *Smed-TRAF-2A/B(RNAi)*, these animals still developed irreversible macroscopic injuries. This may suggest that the high levels of apoptosis could be overwhelming the balance between cell death and cell proliferation. Another possible scenario is that cellular differentiation might be impaired in *Smed-TRAF-1/2; -2A/B(RNAi)* animals or that a combination of both increased levels of cell death and poor differentiation lead to growing morphological defects without the ability to renew damaged tissue.

Previous RNA sequencing (RNA-seq) data predicted TRAF-1 is enriched in the early progeny of neoblasts, which is consistent with a possible role in differentiation (Wurtzel et al., 2015). Consistently, we identified that gene expression for both the early progeny marker *Smed-Prog1* and late progeny marker *Smed-Agat1* were sharply reduced as the phenotype began developing, 5 days after the first injection in *Smed-TRAF-1/2(RNAi)* and *Smed-TRAF-2A/B(RNAi)* animals (Figure 3A). Furthermore, using fluorescent *in situ* hybridization (FISH) with the late progeny marker *Smed-AGAT1*, we were able to visualize empty areas of gene expression that were consistent with tissue damage mostly evident in the anterior end (Figure 3B). We also extended the analysis by measuring gene expression on a panel of differentiation markers across various cell lineages (Zeng et al., 2018; Zhu et al., 2015). Although there were some noticeable increases in expression (e.g., *Smed-mex3*), there was an overall reduction in expression levels across the board (Figure 3C). The results suggest that *Smed-TRAF-1/2* and *Smed-TRAF-2A/B* may participate in both cellular differentiation and survival.

Functional Disruption of TRAF-like Proteins Leads to Abnormalities Resembling the AKT Phenotype in Planarians

The *Smed-TRAF-1/2* and *Smed-TRAF-2A/B* phenotypes are characterized by impaired locomotion, tissue swelling, and blisters that together resemble defects observed in *Smed-AKT(RNAi)* (Peiris et al., 2016b). This prompted us to analyze in more detail the possible relationship between the phenotypes. First, we evaluated whether the impaired movement was due to abnormalities in the spatial distribution of the ventral cilia, by performing immunostaining with an anti-acetylated tubulin antibody. The results revealed that *Smed-TRAF-2A/B(RNAi)* animals displayed reduced signal for the anti-acetylated-tubulin antibody as early as 5 days post-RNAi and worsened as the phenotype progressed (Figure 3D). Expression analysis using markers of ventral cilia flagellar beating revealed generalized reduction in both *Smed-TRAF-2A/B(RNAi)* and in *Smed-TRAF-1/2(RNAi)* animals (Figure 3E). This impaired movement coincided with edema (blisters) and swelling that appears within 5 days after the first injection in *Smed-TRAF-2A/B(RNAi)* animals (Figure 1C). We also found *Smed-AKT* expression was decreased in both *Smed-TRAF-1/2* and *-2A/B(RNAi)* animals (Figure 3F). Likewise, we identified a decrease in protonephridia differentiation marker (*Smed-POU2/3*) and protonephridia groups (distal tubules, proximal tubules, collecting ducts) in both *Smed-TRAF-1/2* and *-2A/B(RNAi)* animals (Figure 3G). Overall, we find that loss of *Smed-TRAF-1/2; -2A/B* resembles defects similar to those observed in *Smed-AKT(RNAi)* animals, suggesting TRAF-like proteins in planarians might be directly or indirectly upstream of *Smed-AKT*.

Loss of *Smed-TRAF-1/2* and *Smed-TRAF-2A/B* Impairs Tissue Regeneration

Planarians have a robust ability to regenerate missing tissue in response to injury (Newmark and Sánchez Alvarado, 2002; Reddien and Alvarado, 2004). Previous reports using RNA-seq data have predicted that TRAF expression is upregulated upon wounding (Sandmann et al., 2011; Wenemoser et al., 2012; Wurtzel

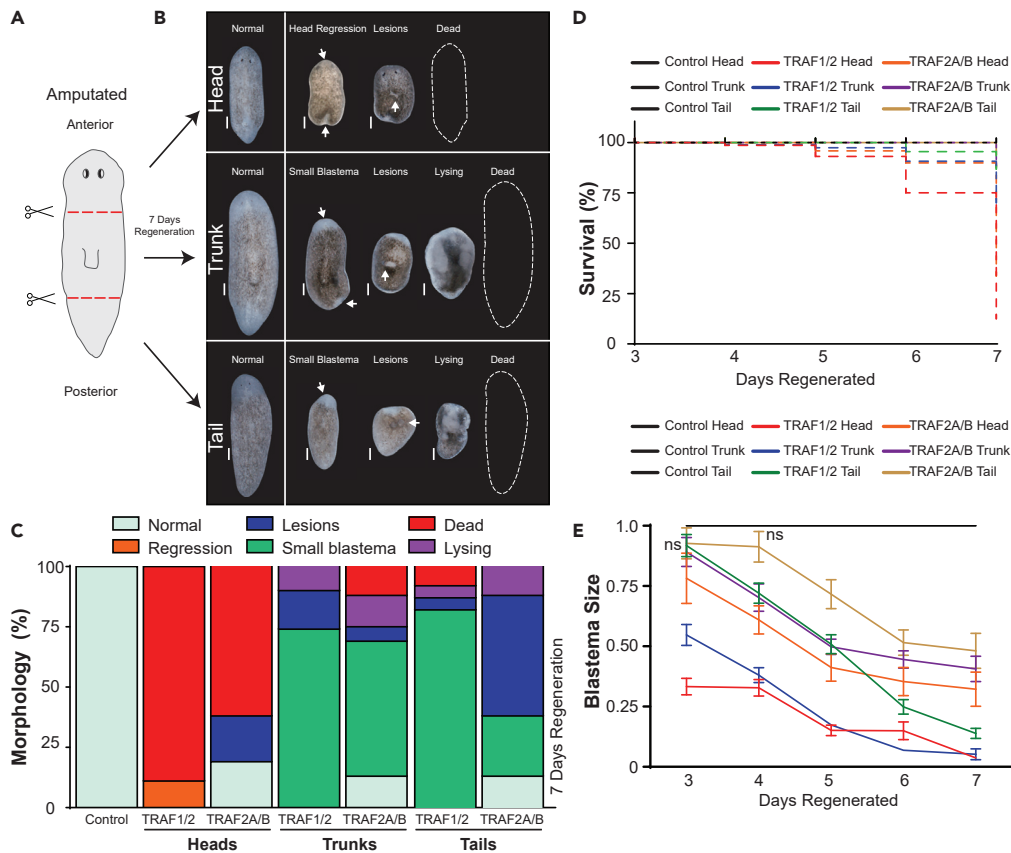


Figure 4. Loss of *Smed-TRAF-1/2* and *Smed-TRAF-2A/B* Impairs Regeneration

(A) Schematic representation for amputation/regeneration experiments.

(B) Live images are depicting the various gross morphological defects observed in regenerating fragments after 7 days. Scale bars, 200 μ m.

(C) Plots are displaying the prevalence of the gross morphology seen in *Smed-TRAF-1/2(RNAi)* and *Smed-TRAF-2A/B(RNAi)* animals after 7 days of regeneration.

(D) Survival plot of regenerating fragments over the length of the time course. Percentage of survival in fragments 7 days post amputation; Control, 100%, *Smed-TRAF-1/2* (Heads, 12%, Trunks, 70%, Tails, 86%), *Smed-TRAF-2A/B* (Heads, 33%, Trunks, 87%, Tails, 93%).

(E) Quantification of regenerated tissue (blastema) in proportion to the area of the animal. Blastema size is represented as fold change compared with control animals. All data points were significant unless denoted (ns); two-way ANOVA. All data were obtained from more than 16 animals with at least two technical replicates. Data are represented as mean \pm SEM.

et al., 2015). However, there are contrasting results about TRAFs function during planarian regeneration (Arnold et al., 2016; Rouhana et al., 2010). Therefore, we set out to test the role of TRAF-like proteins, *Smed-TRAF-1/2* and *Smed-TRAF-2A/B*, during regeneration. To this end, we amputated RNAi animals before the development of any phenotypic manifestations (4 days after the first injection). Animals were amputated at both anterior (pre-pharyngeal) and posterior (post-pharyngeal) regions, and regenerating fragments were observed over 7 days (Figure 4A). Over this regeneration period, *Smed-TRAF-1/2(RNAi)* and *Smed-TRAF-2A/B(RNAi)* animals developed morphological defects, some of which led to the death of animals. It appeared that *Smed-TRAF-1/2(RNAi)* had a more detrimental impact on regenerating head fragments, whereas *Smed-TRAF-2A/B(RNAi)* had a more prominent effect in the regeneration of tail fragments (Figures 4B–4D). The blastema size was also reduced in both *Smed-TRAF-1/2(RNAi)* and *Smed-TRAF-2A/B(RNAi)* animals when compared with control animals (Figure 4E). These results suggest that both *Smed-TRAF-1/2* and *Smed-TRAF-2A/B* are required for proper tissue regeneration.

Next, we evaluated whether reduced blastema size in *Smed-TRAF-1/2(RNAi)* and *Smed-TRAF-2A/B(RNAi)* animals was accompanied by the regeneration of missing organs/tissues. A lack of photoreceptor

pigmentation in the optic cups of newly regenerated anterior tissue in both *Smed-TRAF-1/2(RNAi)* and *Smed-TRAF-2A/B(RNAi)* animals was observed (Figure 4B). This finding led us to believe that both *Smed-TRAF-1/2(RNAi)* and *Smed-TRAF-2A/B(RNAi)* animals displayed impaired nervous system regeneration. Indeed, we discovered that both *Smed-TRAF-1/2(RNAi)* and *Smed-TRAF-2A/B(RNAi)* animals presented abnormal morphology or absent photoreceptors (Figures 5A and 5B). Further analysis revealed a reduction of regenerating brain size in both *Smed-TRAF-1/2(RNAi)* and *Smed-TRAF-2A/B(RNAi)* animals compared with control animals (Figures 5C and 5D). It appeared that *Smed-TRAF1/2(RNAi)* animals had more severe impacts on regeneration, displayed by lower levels of survival, a reduction in blastemal size, and smaller brain size compared with *Smed-TRAF-2A/B(RNAi)* animals.

To gain insights about the mechanisms mediating defective tissue regeneration in *Smed-TRAF-1/2(RNAi)* and *Smed-TRAF-2A/B(RNAi)* animals, we analyzed levels of cell proliferation and death as their stereotypic occurrence is needed during tissue repair (Pellettieri et al., 2010; Wenemoser and Reddien, 2010). We evaluated the levels of Caspase-3 intensity during a 7-day time course in regenerating head, trunk, and tail fragments from both *Smed-TRAF-1/2(RNAi)* and *Smed-TRAF-2A/B(RNAi)* animals. These experiments evidenced increases in cell death for both experimental conditions. However, in *Smed-TRAF-2A/B(RNAi)* animals, the increase in cell death was evident after the second day post amputation in all regenerating fragments (Figures 5E and 5F). The mitotic activity decreased gradually and fell below normal levels as regeneration progressed in each fragment subjected to either *Smed-TRAF-1/2(RNAi)* or *Smed-TRAF-2A/B(RNAi)* (Figures 5G and 5H). Overall, this suggests that *Smed-TRAF-1/2* and *Smed-TRAF-2A/B* are essential for maintaining levels of cellular proliferation and cell death that is required to regenerate missing structures.

DISCUSSION

Our results describe two TRAF-like proteins in *S. mediterranea*, *Smed-TRAF-1/2* and *Smed-TRAF-2A/B*, which have essential roles in cell death, differentiation, and proliferation. We found loss of *Smed-TRAF-1/2* and *Smed-TRAF-2A/B* is followed by an aggressive phenotype characterized by external lesions, blisters, and locomotion impairment, respectively. The phenotypes rapidly progress to a more severe condition involving tissue lysing followed by animal death within 15 days of RNAi. The phenotypes are highly toxic, affecting not only homeostatic cellular turnover but also regeneration. Overall, we find *Smed-TRAF-1/2* and *Smed-TRAF-2A/B* are essential for cellular survival and differentiation.

RNA-seq in the planarian model has led to the identification of several predicted TRAF proteins (Forsthoefel et al., 2019; Grohme et al., 2018; Hu et al., 2019; Pang et al., 2016; Ross et al., 2018; Sandmann et al., 2011; Swapna et al., 2018; Wenemoser et al., 2012; Wurtzel et al., 2015). Most of these predictions are based on the presence of the MATH domains, which are not necessarily specific to the TRAF family and are also present in the USP7, MATH/BTB, MATH/Filament, TRIM37, and Meprin family of proteins (Zapata et al., 2007). Although some of these TRAF proteins have been characterized within the context of regeneration (Rouhana et al., 2010; Sandmann et al., 2011; Wenemoser et al., 2012; Wurtzel et al., 2015) and pathogen defense (Arnold et al., 2016; Pang et al., 2016; Tsoumtsa et al., 2017), morphological defects and toxicity were not previously described. Further analysis will be required to determine the underlying molecular mechanisms by which these planarian TRAF-like proteins are regulated.

TRAF proteins have been identified across various vertebrate and invertebrate species. TRAF4 has been predicted to be one of the oldest members of the TRAF family proteins, whereas TRAF1 and TRAF2 appear as a result of a more recent gene duplication event (Zapata et al., 2007). From our phylogenetic analysis, we find *Smed-TRAF-1/2* and *Smed-TRAF-2A/B* to be distantly related from their vertebrate TRAF counterparts, which is strikingly similar to *D. melanogaster* TRAF proteins. However, the TRAF-like proteins identified in this study showed less divergence to vertebrate TRAF proteins than previously reported (Rouhana et al., 2010; Wurtzel et al., 2015). Although *Smed-TRAF-1/2* and *Smed-TRAF-2A/B* have diverged from their vertebrate counterparts, some of their functionality may have remained intact. For example, vertebrate TRAF1 and TRAF2 have important antiapoptotic roles, which were also present in *Smed-TRAF-1/2* and *Smed-TRAF-2A/B* (Arron et al., 2002).

TRAF-like planarian proteins are critical regulators of cell survival, which is consistent with the survival functions assigned to *Smed-AKT*. We found substantial overlap between the phenotypes in *Smed-TRAFs* and *Smed-AKT*, such as bloating, impaired movement, reduction of cilia distribution, decreased protonephridia, hyperproliferation, and increased cell death. We propose that TRAF-like proteins in *S. mediterranea*

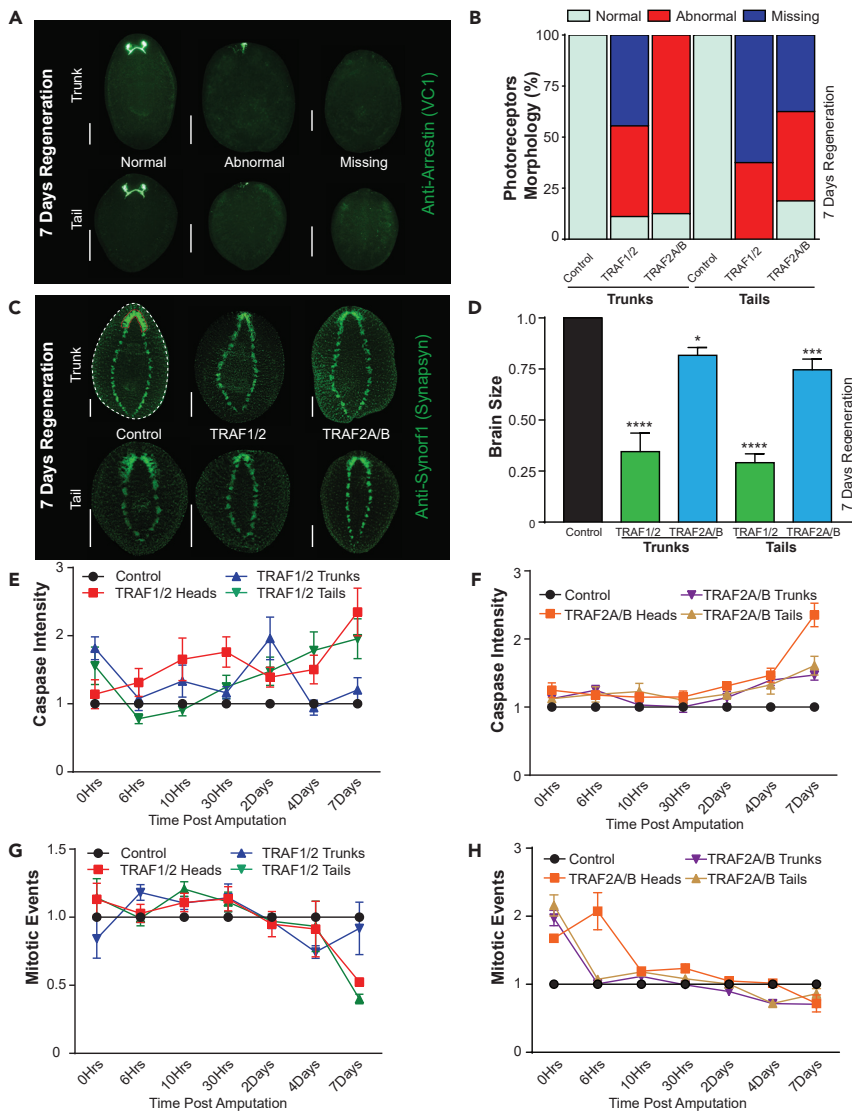


Figure 5. *Smed-TRAF-1/2* and *Smed-TRAF-2A/B* RNAi Disrupts CNS Regeneration and Tissue Turnover

(A) Whole-mount immunohistochemistry using the marker Anti-Arrestin (VC1) antibody to visualize the photoreceptor morphology in regenerating trunk and tail fragments after 7 days of regeneration. Defects in photoreceptors were categorized as abnormal if animals displayed anything less than two completely intact photoreceptors, or missing if there was no staining evident. Scale bars, 200 μ m.

(B) Plots are displaying the distribution of morphology in control, *Smed-TRAF-1/2*(RNAi), and *Smed-TRAF-2A/B*(RNAi) animals represented in (A). Data were obtained from more than eight animals with at least two technical replicates.

(C) Whole-mount immunohistochemistry using the marker Anti-Synorff1 (Synapsyn) antibody to visualize the morphology of the CNS in regenerating trunk and tail fragments after 7 days of regeneration. The area of the brain (red dashed lines) and area of the animal (white dashed lines) were computed from the staining. Scale bar, 200 μ m.

(D) Quantification of brain size, computed from (C) using the area of the spongy region of the cephalic ganglia (red dashed), which was normalized to the area of the whole animal (white dashed). Data were obtained from more than seven animals with at least two technical replicates. * $p < 0.05$; *** $p < 0.001$; **** $p < 0.0001$; one-way ANOVA.

(E and F) Caspase-3 intensity readings in *Smed-TRAF-1/2*(RNAi) and *Smed-TRAF-2A/B*(RNAi) regenerating animals using the Anti-Caspase-3 antibody, represented as fold change for each time point. Data were obtained from more than 15 animals using two technical replicates.

(G and H) The number of mitotic events in *Smed-TRAF-1/2*(RNAi) and *Smed-TRAF-2A/B*(RNAi) regenerating animals using the Anti-Phospho-histone H3 (serine-10) (H3P) antibody, represented as fold change for each time point. Data were obtained from more than 15 animals using two technical replicates. Data are represented as mean \pm SEM.

may act upstream of AKT signaling. This may be an evolutionarily conserved feature observed in TRAF2 overexpression that leads to enhanced hypertrophy through the activation of AKT/GSK3 β signaling (Huang et al., 2014). Although *Smed-AKT* and *Smed-TRAFs* share many similarities, the progression of the phenotype is extremely rapid in *Smed-TRAF(RNAi)* animals (15 days RNAi) compared with *Smed-AKT(RNAi)* animals (45 days RNAi). We also find the bloating phenotype of *Smed-TRAF-2A/B(RNAi)* animals appear in the mid-section of the animals, whereas *Smed-AKT(RNAi)* produce a bloated tail region, with an elongation of the head portion (Peiris et al., 2016b). It is challenging to predict whether AKT is a direct target of *Smed-TRAF-1/2* and *-2A/B* genes in planarians. Further analysis using antibodies specific for phosphorylation of AKT could elucidate biochemical regulation by both *Smed-TRAF-1/2* and *Smed-TRAF-2A/B*.

TRAF proteins play essential roles with stress and immune responses (Arch et al., 1998; Honda and Taniguchi, 2006). Exposure of irradiation in planarians causes DNA double-strand breaks, which is a known cellular stressor (Barghouth et al., 2019; Peiris et al., 2016a). We uncovered that exposure to ionizing radiation increases the expression for both *Smed-TRAF-1/2* and *Smed-TRAF-2A/B*, which is consistent with previous findings on TRAF signaling using *S. mediterranea* and *Dugesia japonica* (Rouhana et al., 2010; Wenemoser et al., 2012). Likewise, wounding induces a form of systemic stress accompanied by cascades of wound response genes in planarians (Wurtzel et al., 2015). And the expression of TRAF homologs is increased upon wounding (Sandmann et al., 2011; Wenemoser et al., 2012; Wurtzel et al., 2015). Our results support that both *Smed-TRAF-1/2* and *Smed-TRAF-2A/B* were required for proper regeneration. Similar observations were found in *DjTraf-2a(RNAi)* animals, in which they developed small heads, abnormal pigment cups, and photoreceptors, accompanied by lack of tail regeneration (Rouhana et al., 2010). Planarians are emerging as a valuable model to study host-pathogen interactions because they show extraordinary capacity to clear infection by pathogenic bacteria and fungi (Abnave et al., 2014; Arnold et al., 2016; Gao et al., 2017; Hammoudi et al., 2018; Li et al., 2019; Lu et al., 2017; Maciel et al., 2019; Pang et al., 2016; Torre et al., 2017; Tsoumtsa et al., 2017). Recent studies identified *Smed-Traf-6* expression increases upon exposure to *S. aureus* and synthetic toll-like receptor (TRL) ligands, lipopolysaccharide (LPS), and peptidoglycan (PGN) (Pang et al., 2016; Tsoumtsa et al., 2017). Likewise, disturbance of the putative *Smed-Traf-2* leads to increased pathological defects when infected with pseudomonas (Arnold et al., 2016). Together, TRAF signaling in planarians appears as a generalized mediator of stress responses under different circumstances. However, further analysis would be required to determine how TRAFs signaling mechanistically regulate these responses in planarians.

Limitations of the Study

We find that loss of both *Smed-TRAF-1/2* and *Smed-TRAF-2A/B* leads to rapid toxicity. Therefore, we are unable to discriminate if early death is due to failure of overall cellular differentiation or merely an overwhelming surge in cell death. Further biochemical and genomic analyses, along with lineage tracing and early detection in cellular survival markers would facilitate gaining insights about the fundamental mechanisms of planarian TRAF-like protein function.

Resource Availability

Lead Contact

Further information and requests for resources and reagents should be directed to and fulfilled by the Lead Contact, Néstor J. Oviedo: noviedo2@ucmerced.edu.

Materials Availability

All sequences used to perform *in situ* hybridization and quantitative real-time PCR were provided in [Table S1](#) and [S2](#), [Transparent Methods](#) supplemental file.

Data and Code Availability

This study did not generate datasets or code.

METHODS

All methods can be found in the accompanying [Transparent Methods](#) supplemental file.

SUPPLEMENTAL INFORMATION

Supplemental Information can be found online at <https://doi.org/10.1016/j.isci.2020.101665>.

ACKNOWLEDGMENTS

We thank Edelweiss Pfister for technical assistance and members of the Oviedo lab at UC Merced for their comments on the manuscript. We thank Drs. Chris Amemiya and Daniel Ocampo-Daza for comments on phylogenetic analysis. We thank Dr. K. Watanabe for VC-1 antibody. The SYNORF antibody developed by Dr. E. Buchner at the ICNUW was obtained from the Developmental Studies Hybridoma Bank, created by the NICHD of the NIH and maintained at the University of Iowa, Department of Biology. Confocal images were obtained in a microscope supported by the National Science Foundation grant number DMR-1625733. This work was supported by the University of California Cancer Research Coordinating Committee (Award# CRR-18-525108) and the National Institutes of Health (NIH) National Institute of General Medical Sciences (NIGMS) award R01GM132753 to N.J.O.

AUTHOR'S CONTRIBUTIONS

Conceptualization, B.Z., P.G.B., E.I.M.; Methodology and Formal Analysis, B.Z., P.G.B., E.I.M.; Investigation, B.Z., P.G.B., E.I.M.; Writing – Original Draft, B.Z., P.G.B., E.I.M., N.J.O.; Writing – Review & Editing, B.Z., P.G.B., E.I.M., N.J.O.; Funding Acquisition, N.J.O.; Resources, N.J.O.; Supervision, N.J.O.

DECLARATION OF INTERESTS

The authors declare no competing interests.

Received: May 16, 2020

Revised: July 31, 2020

Accepted: October 7, 2020

Published: November 20, 2020

REFERENCES

- Abnave, P., Mottola, G., Gimenez, G., Boucherit, N., Trouplin, V., Torre, C., Conti, F., Ben Amara, A., Lepolard, C., Djian, B., et al. (2014). Screening in planarians identifies MORN2 as a key component in LC3-associated phagocytosis and resistance to bacterial infection. *Cell Host Microbe* 16, 338–350.
- Arch, R.H., Gedrich, R.W., and Thompson, C.B. (1998). Tumor necrosis factor receptor-associated factors (TRAFs)—a family of adapter proteins that regulates life and death. *Genes Dev.* 12, 2821–2830.
- Arkee, T., and Bishop, G.A. (2019). TRAF family molecules in T cells: multiple receptors and functions. *J. Leukoc. Biol.* 107, 907–915, 2MR1119-397R.
- Arnold, C.P., Merryman, M.S., Harris-Arnold, A., McKinney, S.A., Seidel, C.W., Loethen, S., Proctor, K.N., Guo, L., and Sánchez Alvarado, A. (2016). Pathogenic shifts in endogenous microbiota impede tissue regeneration via distinct activation of TAK1/MKK/p38. *Elife* 5, e16793.
- Arron, J.R., Pewzner-Jung, Y., Walsh, M.C., Kobayashi, T., and Choi, Y. (2002). Regulation of the subcellular localization of tumor necrosis factor receptor-associated factor (TRAF2) by TRAF1 reveals mechanisms of TRAF2 signaling. *J. Exp. Med.* 196, 923–934.
- Barghouth, P.G., Thiruvalluvan, M., LeGro, M., and Oviedo, N.J. (2019). DNA damage and tissue repair: what we can learn from planaria. *Semin. Cell Dev. Biol.* 87, 145–159.
- Bishop, G.A., Abdul-Sater, A.A., and Watts, T.H. (2019). Editorial: TRAF proteins in Health and disease. *Front. Immunol.* 10, 326.
- Castillo-Lara, S., and Abril, J.F. (2018). PlanNET: homology-based predicted interactome for multiple planarian transcriptomes. *Bioinformatics* 34, 1016–1023.
- Chiffolleau, E., Kobayashi, T., Walsh, M.C., King, C.G., Walsh, P.T., Hancock, W.W., Choi, Y., and Turka, L.A. (2003). TNF receptor-associated factor 6 deficiency during hemopoiesis induces Th2-polarized inflammatory disease. *J. Immunol.* 171, 5751–5759.
- Deshaies, R.J., and Joazeiro, C.A.P. (2009). RING domain E3 ubiquitin ligases. *Annu. Rev. Biochem.* 78, 399–434.
- Elliott, S.A., and Sánchez Alvarado, A. (2013). The history and enduring contributions of planarians to the study of animal regeneration. *Wiley Interdiscip. Rev. Dev. Biol.* 2, 301–326.
- Forsthoefel, D.J., Cejda, N.I., Khan, U.W., and Newmark, P.A. (2019). Cell-type diversity and regionalized gene expression in the planarian intestine revealed by laser-capture microdissection transcriptome profiling (preprint). *Dev. Biol.* <https://doi.org/10.1101/756924>.
- Gao, L., Han, Y., Deng, H., Hu, W., Zhen, H., Li, N., Qin, N., Yan, M., Wu, W., Liu, B., et al. (2017). The role of a novel C-type lectin-like protein from planarian in innate immunity and regeneration. *Dev. Comp. Immunol.* 67, 413–426.
- Grohme, M.A., Schloissnig, S., Rozanski, A., Pippel, M., Young, G.R., Winkler, S., Brandl, H., Henry, I., Dahl, A., Powell, S., et al. (2018). The genome of *Schmidtea mediterranea* and the evolution of core cellular mechanisms. *Nature* 554, 56–61.
- Hammoudi, N., Torre, C., Ghigo, E., and Drancourt, M. (2018). Temperature affects the biology of *Schmidtea mediterranea*. *Sci. Rep.* 8, 14934.
- Honda, K., and Taniguchi, T. (2006). IRFs: master regulators of signalling by Toll-like receptors and cytosolic pattern-recognition receptors. *Nat. Rev. Immunol.* 6, 644–658.
- Hu, W., Wu, W., Sun, S., Liu, Z., Li, A., Gao, L., Liu, X., Liu, D., Deng, H., Zhao, B., et al. (2019). Identification and characterization of a TNF receptor-associated factor in *Dugesia japonica*. *Gene* 681, 52–61.
- Huang, Y., Wu, D., Zhang, X., Jiang, M., Hu, C., Lin, J., Tang, J., and Wu, L. (2014). Cardiac-specific Traf2 overexpression enhances cardiac hypertrophy through activating AKT/GSK3 β signaling. *Gene* 536, 225–231.
- Karin, M., Liu, Z.G., and Zandi, E. (1997). AP-1 function and regulation. *Curr. Opin. Cell Biol.* 9, 240–246.
- Li, N., Li, A., Zheng, K., Liu, X., Gao, L., Liu, D., Deng, H., Wu, W., Liu, B., Zhao, B., and Pang, Q. (2019). Identification and characterization of an atypical RIG-I encoded by planarian *Dugesia japonica* and its essential role in the immune response. *Dev. Comp. Immunol.* 91, 72–84.
- Lomaga, M.A., Yeh, W.C., Sarosi, I., Duncan, G.S., Furlonger, C., Ho, A., Morony, S., Capparelli, C., Van, G., Kaufman, S., et al. (1999). TRAF6 deficiency results in osteopetrosis and defective interleukin-1, CD40, and LPS signaling. *Genes Dev.* 13, 1015–1024.
- Lu, Q., Wu, S., Zhen, H., Deng, H., Song, Q., Ma, K., Cao, Z., Pang, Q., and Zhao, B. (2017). 14-3-3 α

and 14-3-3 ζ contribute to immune responses in planarian *Dugesia japonica*. *Gene* 615, 25–34.

Maciel, E.I., Jiang, C., Barghouth, P.G., Nobile, C.J., and Oviedo, N.J. (2019). The planarian *Schmidtea mediterranea* is a new model to study host-pathogen interactions during fungal infections. *Dev. Comp. Immunol.* 93, 18–27.

Newmark, P.A., and Sánchez Alvarado, A. (2002). Not your father's planarian: a classic model enters the era of functional genomics. *Nat. Rev. Genet.* 3, 210–219.

Nicholson, D.W., and Thornberry, N.A. (1997). Caspases: killer proteases. *Trends Biochem. Sci.* 22, 299–306.

Pang, Q., Gao, L., Hu, W., An, Y., Deng, H., Zhang, Y., Sun, X., Zhu, G., Liu, B., and Zhao, B. (2016). De novo transcriptome analysis provides insights into immune related genes and the RIG-I-like receptor signaling pathway in the freshwater planarian (*Dugesia japonica*). *PLoS One* 11, e0151597.

Park, H.H. (2018). Structure of TRAF family: current understanding of receptor recognition. *Front. Immunol.* 9, 1999.

Peiris, T.H., Hoyer, K.K., and Oviedo, N.J. (2014). Innate immune system and tissue regeneration in planarians: an area ripe for exploration. *Semin. Immunol.* 26, 295–302.

Peiris, T.H., Ramirez, D., Barghouth, P.G., Ofaha, U., Davidian, D., Weckerle, F., and Oviedo, N.J. (2016a). Regional signals in the planarian body guide stem cell fate in the presence of genomic instability. *Development* 143, 1697–1709.

Peiris, T.H., Ramirez, D., Barghouth, P.G., and Oviedo, N.J. (2016b). The Akt signaling pathway is required for tissue maintenance and regeneration in planarians. *BMC Dev. Biol.* 16, 7.

Peiris, T.H., Weckerle, F., Ozamoto, E., Ramirez, D., Davidian, D., García-Ojeda, M.E., and Oviedo, N.J. (2012). TOR signaling regulates planarian stem cells and controls localized and organismal growth. *J. Cell. Sci.* 125, 1657–1665.

Pellettieri, J., Fitzgerald, P., Watanabe, S., Mancuso, J., Green, D.R., and Sánchez Alvarado, A. (2010). Cell death and tissue remodeling in planarian regeneration. *Dev. Biol.* 338, 76–85.

Piva, R., Belardo, G., and Santoro, M.G. (2006). NF- κ B: a stress-regulated switch for cell survival. *Antioxid. Redox Signal.* 8, 478–486.

Reddien, P.W., and Alvarado, A.S. (2004). Fundamentals OF planarian regeneration. *Annu. Rev. Cell Dev. Biol.* 20, 725–757.

Ross, K.G., Molinaro, A.M., Romero, C., Dockter, B., Cable, K.L., Gonzalez, K., Zhang, S., Collins, E.-M.S., Pearson, B.J., and Zayas, R.M. (2018). SoxB1 activity regulates sensory neuron regeneration, maintenance, and function in planarians. *Dev. Cell* 47, 331–347.e5.

Rouhana, L., Shibata, N., Nishimura, O., and Agata, K. (2010). Different requirements for conserved post-transcriptional regulators in planarian regeneration and stem cell maintenance. *Dev. Biol.* 341, 429–443.

Rozanski, A., Moon, H., Brandl, H., Martín-Durán, J.M., Grohme, M.A., Hüttner, K., Bartscherer, K., Henry, I., and Rink, J.C. (2019). PlanMine 3.0—improvements to a mineable resource of flatworm biology and biodiversity. *Nucleic Acids Res.* 47, D812–D820.

Sandmann, T., Vogg, M.C., Owlarn, S., Boutros, M., and Bartscherer, K. (2011). The head-regeneration transcriptome of the planarian *Schmidtea mediterranea*. *Genome Biol.* 12, R76.

Swapna, L.S., Molinaro, A.M., Lindsay-Mosher, N., Pearson, B.J., and Parkinson, J. (2018). Comparative transcriptomic analyses and single-cell RNA sequencing of the freshwater planarian *Schmidtea mediterranea* identify major cell types and pathway conservation. *Genome Biol.* 19, 124.

Thiruvalluvan, M., Barghouth, P.G., Tsur, A., Broday, L., and Oviedo, N.J. (2018). SUMOylation controls stem cell proliferation and regional cell death through Hedgehog signaling in planarians. *Cell. Mol. Life Sci.* 75, 1285–1301.

Torre, C., Abnave, P., Tsoumtsas, L.L., Mottola, G., Lepolard, C., Trouplin, V., Gimenez, G., Desrousseaux, J., Gempp, S., Levasseur, A., et al. (2017). *Staphylococcus aureus* promotes Smed-PGRP-2/Smed-setd8-1 methyltransferase signalling in planarian neoblasts to Sensitize anti-bacterial gene responses during Re-infection. *EBioMedicine* 20, 150–160.

Tsoumtsas, L.L., Torre, C., Trouplin, V., Coiffard, B., Gimenez, G., Mege, J.-L., and Ghigo, E. (2017). Antimicrobial capacity of the freshwater planarians against *S. aureus* is under the control of Timeless. *Virulence* 8, 1160–1169.

Tu, K.C., Cheng, L.-C., T K Vu, H., Lange, J.J., McKinney, S.A., Seidel, C.W., and Sánchez Alvarado, A. (2015). Egr-5 is a post-mitotic regulator of planarian epidermal differentiation. *Elife* 4, e105011.

Wenemoser, D., Lapan, S.W., Wilkinson, A.W., Bell, G.W., and Reddien, P.W. (2012). A molecular wound response program associated with regeneration initiation in planarians. *Genes Dev.* 26, 988–1002.

Wenemoser, D., and Reddien, P.W. (2010). Planarian regeneration involves distinct stem cell responses to wounds and tissue absence. *Dev. Biol.* 344, 979–991.

Wurtzel, O., Cote, L.E., Poirier, A., Satija, R., Regev, A., and Reddien, P.W. (2015). A generic and cell-type-specific wound response precedes regeneration in planarians. *Dev. Cell* 35, 632–645.

Xie, P. (2013). TRAF molecules in cell signaling and in human diseases. *J. Mol. Signal.* 8, 7.

Xu, Y., Cheng, G., and Baltimore, D. (1996). Targeted disruption of TRAF3 leads to postnatal lethality and defective T-dependent immune responses. *Immunity* 5, 407–415.

Yang, X.-D., and Sun, S.-C. (2015). Targeting signaling factors for degradation, an emerging mechanism for TRAF functions. *Immunol. Rev.* 266, 56–71.

Yeh, W.C., Shahinian, A., Speiser, D., Kraunus, J., Billia, F., Wakeham, A., de la Pompa, J.L., Ferrick, D., Hum, B., Iscove, N., et al. (1997). Early lethality, functional NF- κ B activation, and increased sensitivity to TNF-induced cell death in TRAF2-deficient mice. *Immunity* 7, 715–725.

Zapata, J.M., Martínez-García, V., and Lefebvre, S. (2007). Phylogeny of the TRAF/MATH domain. *Adv. Exp. Med. Biol.* 597, 1–24.

Zapata, J.M., Pawlowski, K., Haas, E., Ware, C.F., Godzik, A., and Reed, J.C. (2001). A diverse family of proteins containing tumor necrosis factor receptor-associated factor domains. *J. Biol. Chem.* 276, 24242–24252.

Zeng, A., Li, H., Guo, L., Gao, X., McKinney, S., Wang, Y., Yu, Z., Park, J., Semerad, C., Ross, E., et al. (2018). Prospectively isolated tetraspanin + neoblasts are adult pluripotent stem cells underlying planaria regeneration. *Cell* 173, 1593–1608.e20.

Zhu, S.J., Hallows, S.E., Currie, K.W., Xu, C., and Pearson, B.J. (2015). A mex3 homolog is required for differentiation during planarian stem cell lineage development. *Elife* 4, e07025.

Ziman, B., Karabinis, P., Barghouth, P., and Oviedo, N.J. (2020). Sirtuin-1 regulates organismal growth by altering feeding behavior and intestinal morphology in planarians. *J. Cell Sci.* 133, 239467.

iScience, Volume 23

Supplemental Information

TRAF-like Proteins Regulate Cellular Survival in the Planarian *Schmidtea mediterranea*

Benjamin Ziman, Paul G. Barghouth, Eli Isael Maciel, and Néstor J. Oviedo

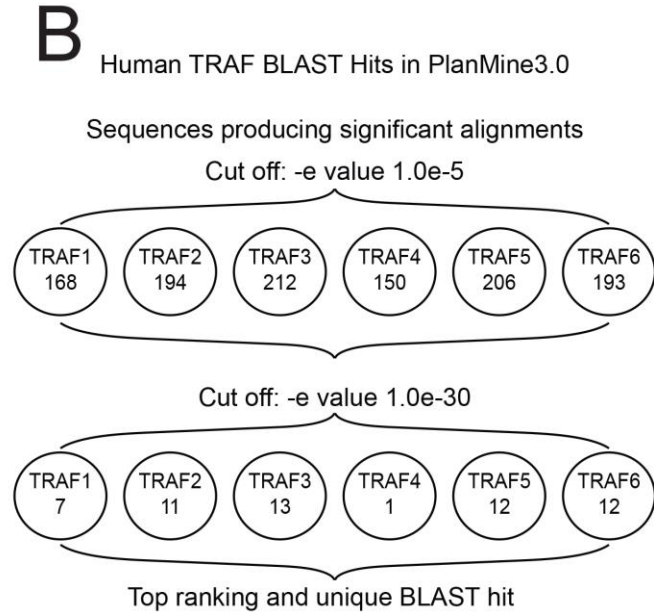
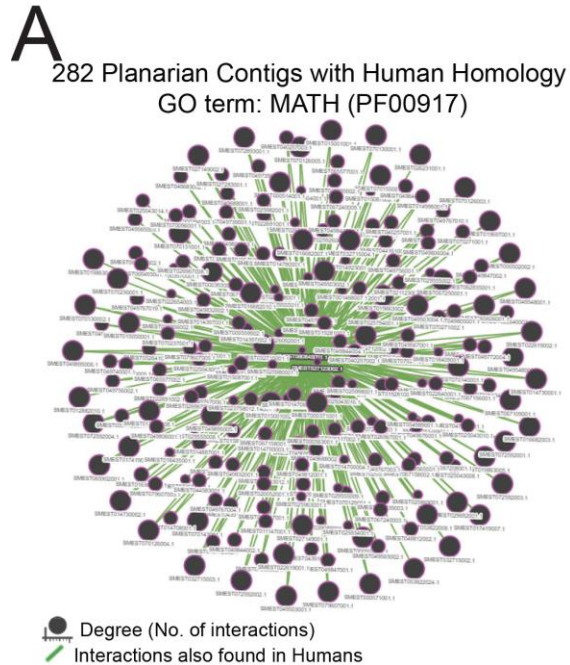


Figure S1. Identification of planarian TRAF-like proteins. A) An interaction map of predicted genes possessing MATH domains. Interactions are represented by the degree or number of interactions (size of purple circles) interactions that are found between predicted planarians genes in their human counterparts (green lines). **B)** The process used to identify TRAF proteins in the planarian model. Human TRAF protein sequences were blasted into the planarian database (Planmine3.0), the number of predicted genes was filtered down based on the cut off for the $-e$ value parameters set (1.0e-5 followed by 1.0e-30). The top-ranked predicted sequence was selected.

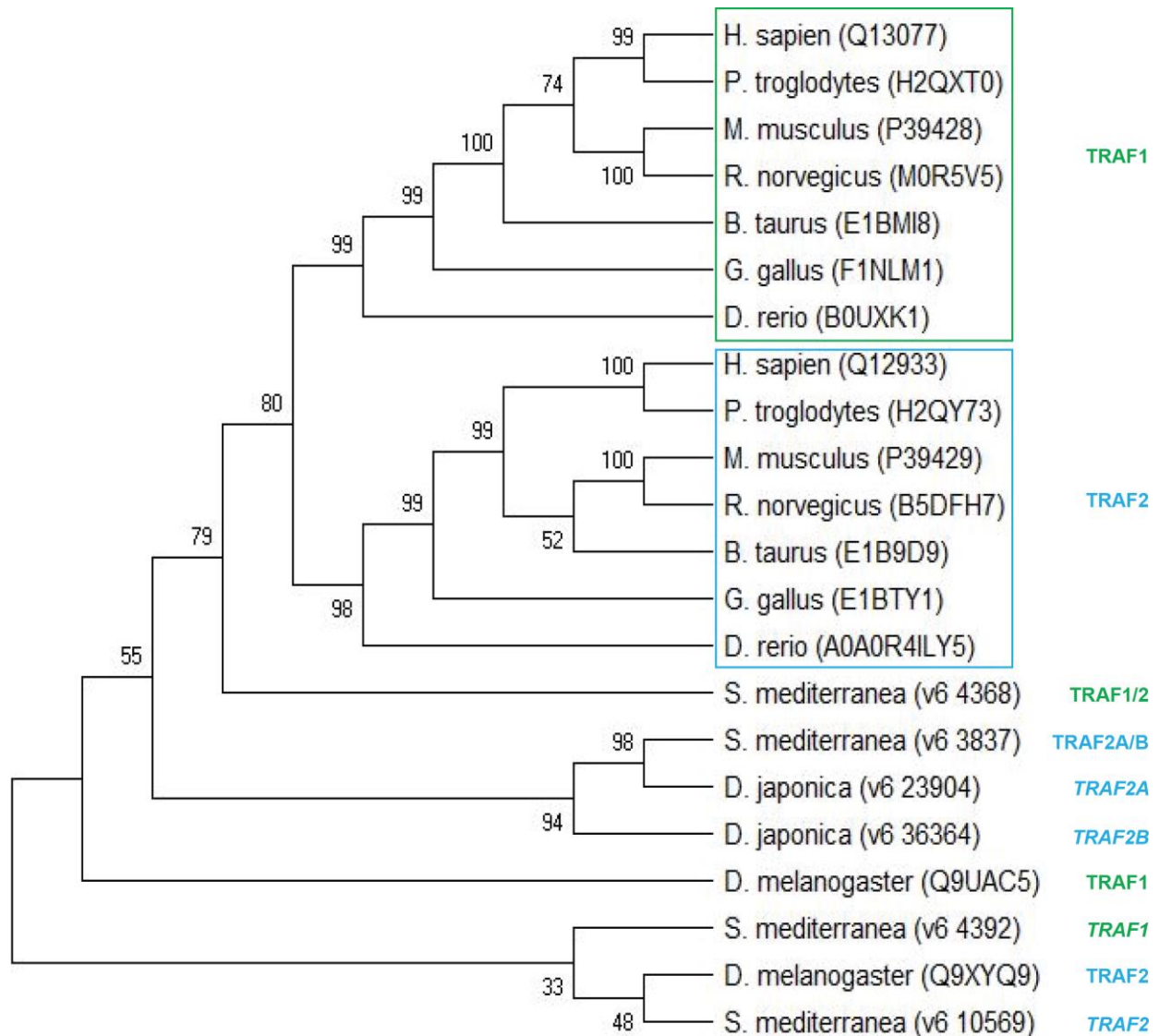


Figure S2. Phylogenetic tree construction for TRAF homologs. Phylogenetic bootstrap consensus tree of TRAF1 and TRAF2 homologs across various phyla. Previously published TRAF proteins are represented with italic labels. A phylogenetic tree was constructed applying the maximum likelihood method with a boot strap consensus from 500 replicates using MegaX software.

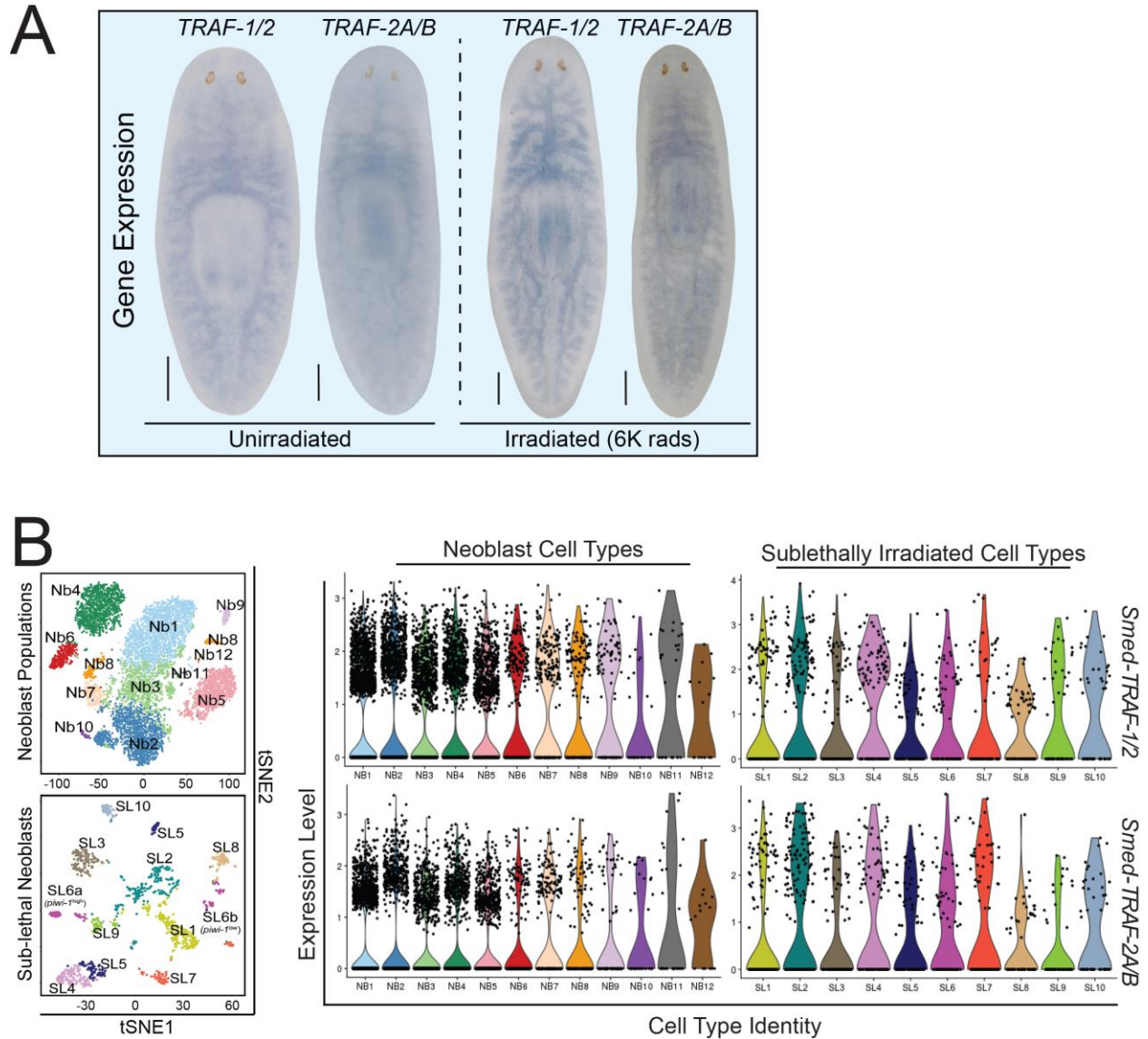


Figure S3. Expression patterns of planarian TRAF-like proteins. A) Whole-mount *in situ* hybridization using antisense probes for *Smed-TRAF-1/2* and *Smed-TRAF-2A/B*, 24 hours after lethal (6K rad) irradiation (right). Scale bars = 200 μ m. **B)** Expression levels for *Smed-TRAF-1/2*, and *-2A/B* determined using the Planosphere fate mapping atlas (Zeng et al., 2018). *Smed-TRAF-1/2* and *Smed-TRAF-2A/B* appear to be significantly distributed across all neoblast and sub-lethally irradiated cell clusters.

Table S1: Primer sequences used for cloning and making riboprobes for *in situ* hybridization related to Figure 1 and Figure S3.

Primer Name	Sequence
<i>Smed-TRAF-1/2</i>	Forward primer: TTGGCAGGTGAGATCAAAGCA Reverse primer: GCTGCCAGAAGGGATGTTCA
<i>Smed-TRAF-2A/B</i>	Forward primer: TAGCAAATGGACCGAAGCCT Reverse primer: GAATCGGGGTTGGGAAGGAT

Table S2: Primer sequences used for transcript analysis related to Figure 3

Primer Name	Sequence
<i>BCL2</i>	Forward primer: TGGTAGAAGCTCAAGACCGTG Reverse primer: ACTCTGGACCACCGTATACAA
<i>NB211.1E</i>	Forward primer: GCAGATGACGTGAAACAAGG Reverse primer: TACTTGATTTGGCGGGAGAC
<i>AGAT1</i>	Forward primer: ACCGATTCCAGTTTCGCTTA Reverse primer: TCAATCGCTCCAAAATCTCA
<i>ODC1</i>	Forward primer: CAAAGTATTGGCCGCAAGCAA Reverse primer: TTCGCTTACGCTCTGAGTTC
<i>PC2</i>	Forward primer: CCCCATGGGTACGACTTCTAT Reverse primer: TCCTCTTGTGGAATCGTCATC
<i>POU2/3</i>	Forward primer: TCGGGTTAGCCCTCGGTAAT Reverse primer: TCGGCTTCTTGCAACCACTT
<i>ATOH8</i>	Forward primer: CTTACCAGAGAACGCCGAGT Reverse primer: AATAACCAGGCACAGCATGGC
<i>ASCL1</i>	Forward primer: AAAACGGGTGGAACAGGTCA Reverse primer: TCAATCGCGACTCTCAAAGTT
<i>GST1</i>	Forward primer: TGTTGCACGAAAACATGGGT Reverse primer: TTATCCCGACCAGAGGTTGC
<i>MEX3</i>	Forward primer: CCCTACACCACCATTCCAACA Reverse primer: TGTGAAAAGTGACGCGGAGT
<i>IC2</i>	Forward primer: GCTGTCCAATCACCGACTGT Reverse primer: ACCGGCTGATAAGATCGCTG
<i>LC1</i>	Forward primer: CATGCGTGCGAAAAATTGTCA Reverse primer: GTTTCTCCGACTGCCTCCAA
<i>AKT</i>	Forward primer: GAGAACTGAAACCGGAACCA Reverse primer: CCCAAATGTTCTTTGCCTA
<i>Slc4A-6</i>	Forward primer: AGAGGCGTTGTCAGTCCAAG Reverse primer: GTCCCTCTGCTCGAATTGGT
<i>Slc6A-13</i>	Forward primer: TCCTGTATAGGCGTCGCAGT Reverse primer: AGAAATGCGCCTCCTCCATT
<i>Slc9A-3</i>	Forward primer: TGATGGAGTTGCAGTGGTGT Reverse primer: ATTGCCATTGTGCATGCGAG
<i>Smed-TRAF1/2</i>	Forward primer: AACAGGTGTGGCCATGAGTT Reverse primer: TGTTTCATGTCTGTCCGTGGT
<i>Smed-TRAF2A/B</i>	Forward primer: TCAGCCACACGTCAAATCTCA Reverse primer: GAATCGGGGTTGGGAAGGAT
<i>TATABOXP</i>	Forward primer: GCAGCGAGAAAGTTTGCCAG Reverse primer: TGTAGCAAACCTGGGTGTGTGA

UDP GLUCOSE

Forward primer: TTCCTACAGCCACTTGAGCGAC

Reverse primer: GTCGGTGGTTATTTGCG

Transparent Methods

Planarian culture

All experiments were carried out using the planarian species *Schmidtea mediterranea*, CIW4 asexual strain. Planarian colonies were maintained as previously described (Oviedo et al., 2008a).

Identification of homologs and phylogenetics

TRAF proteins were identified by blasting in the human TRAF protein sequences into the available planarian databases, PlanMine and PlanNET (Brandl et al., 2016; Castillo-Lara and Abril, 2018; Rozanski et al., 2019). These sequences IDs for *Smed-TRAF-1/2 and 2A/B* (dd_Smed-v6_4368_0_1, dd_Smed-v6_3837_0_1, \ respectively). Protein conservation and identity to human homologs were determined by Clustal Omega and NCBI Conserved domains (<https://www.ncbi.nlm.nih.gov/Structure/cdd/wrpsb.cgi>). A predictive phylogenetic used top hits for TRAF (1 and 2) homologs across various species, obtained using HomoloGene (www.ncbi.nlm.nih.gov/homologene). Previously published planarian TRAF proteins were also included, these included: TRAF-1 (v6_4392), TRAF-2 (v6_10569), TRAF2A (v4_23904), and TRAF2B (v4_36364) (Rouhana et al., 2010; Wurtzel et al., 2015). These confirmed TRAF sequences were aligned by CLUSTALW (MEGA-X software). A phylogenetic bootstrap tree was constructed using the maximum likelihood method, with a consensus of 500 replicates. The tree was produced using MEGA-X software (www.megasoftware.net).

RNAi Experiments

All RNAi experiments were performed on animals starving for at least one week. Cloning of TRAF-like proteins was performed using the TOPO cloning kit (Invitrogen, 450030). Topo vectors possessing individual TRAF-like protein sequences were used to create PCR products with the aid of primers specific for the T3/T7 promoters. The production of dsRNA using PCR

products was carried out using polymerases specific for the T3/T7 promoters regions (Thermo Fisher, FEREP0103, and FEREP0111) as previously described (Oviedo et al., 2008b).

Microinjections were performed as described in Figure 1-B. All microinjections were delivered as 3 pulses (~35nL/pulse) into the gut branch, located in the pre-pharyngeal region of the animals (anterior to the pharynx). All control animals were injected with GFP dsRNA.

Whole-mount *In Situ* Hybridization

Riboprobes were synthesized using T3 or T7 polymerases (Thermo Fisher, FEREP0103, and FEREP0111) and digoxigenin-labeled ribonucleotide mix (Roche, 11277073910) using PCR specific templates (Pearson et al., 2009). Fluorescence *in situ* hybridization and Whole-mount *in situ* hybridization were performed as described previously (King and Newmark, 2013). See Table S1 for probe sequences. Images were taken with the use of the Nikon AZ-100 multizoom microscope and NIS Elements AR 3.2 software.

Protein extraction

Animals were placed into 1.5mL centrifuge tubes with 150 μ L of 1X RIPA Buffer (Cell Signaling Technologies, 9806). 1X RIPA buffer contained protease inhibitors: Complete Mini Protease Inhibitor Cocktail (Roche, 04693124001); 1mM PMSF; 1mM DTT. Samples were homogenized using a motorized pestle (Fisher, 12-141-361) for 10 seconds on ice. Samples were incubated on ice for 45 minutes and then centrifuged at 20,817 g for 20 minutes at 4°C. The supernatant was carefully removed and transferred into a clean tube and placed on ice. Protein concentration was determined using a Bradford protein assay (VWR, E530-1L). The supernatant was mixed with 6X Laemmli buffer (6% SDS, 9% β -mercaptoethanol, 4.8% glycerol, 0.03% bromophenol blue, 375mM Tris-HCl) and incubated at 94°C for 10 minutes to denature and reduce.

Western blot

A total of 50ug of protein lysate were loaded into a 15% SDS-PAGE gel in addition to a molecular weight marker (Thermo Scientific, 26619). Samples were transferred to a methanol-activated (60 seconds) PVDF membrane (Bio-Rad,162-0175) for 1 hour at 55 V in a 1X Tris-glycine transfer buffer[25mM Tris base, 192mM glycine,10%(v/v) methanol] at on ice at 4°C. The membrane was blocked with 5% BSA in TBST [20mM Tris-base, pH 7.6, 140mM NaCl, 0.1%Tween-20] for 2 hours and incubated in the primary antibodies for 16 hours at 4°C on a rocker. The primary antibodies used were, anti-Actin (1:3000; Developmental Studies Hybridoma Bank, JLA20), anti-caspase-3(1:500; Abcam, ab13847). The membrane was washed with TBST four times for 20 minutes before the addition of the secondary antibodies: goat-anti-rabbit HRP IgG antibody (1:4000; Abcam, ab7097) for anti-caspase-3, goat-anti-mouse HRP IgG antibody (1:10000; Invitrogen, G-21040) for anti-Actin. Secondary antibodies were incubated for 1 hour at room temperature with 5% non-fat milk in TBST-SDS [20mM Tris-base, pH 7.6, 140mM NaCl, 0.2%Tween-20, 0.01% SDS]. The membrane was washed four times for 20 minutes with TBST, followed by two times for 5 minutes with 1X PBS. HRP Chemiluminescence substrate allowed for the detection of a signal (Millipore, WBLUF0100A). Blots were stripped for 15min following Caspase-3 detection (Thermo Scientific, 21059) and washed for 20min with 1XPBS before blocking for Actin. Band intensity quantifications were performed by computing the area under the curve, using ImageJ. Caspase-3 activity was normalized to Actin.

Blastema/Brain measurements

Animals were amputated into three fragments (Pre-pharyngeal, Trunk, or Post-Pharyngeal) four days after the first injection. Bright-field images were taken using a Nikon AZ-100 multizoom microscope with NIS Elements AR 3.2 software. Whole animal area and blastema/brain area measurements were calculated using ImageJ. The size of the blastema/brain was normalized to the area (mm²) of the whole animal.

Whole-mount immunofluorescence

Animals were killed, and mucus was removed with 5.7% HCl solution for 5 minutes and then fixed in Carnoy's solution for 2 hours on ice. Carnoy's solution was removed and replaced with 100% MeOH and animals were placed in -20°C for 1 hour. Animals were bleached overnight in MeOH containing 6% H₂O₂. Animals were then rehydrated back to PBSTx [1X PBS, 0.3% Triton-x100]. Animals were blocked for 4 hours in PBSTxB [PBSTx, 0.25% BSA] Primary antibodies: anti- α -Ac-Tubulin (1:500; Sigma, clone 6-11B-1), anti-H3P (1:500; Millipore Cat#05-817R), anti-caspase-3 (1:500; Abcam, ab13847), anti-Arrestin (VC-1) (1:800) a gift from the Watanabe Lab, anti-Synorf1 (Synapsyn) (1:800; Developmental Studies Hybridoma Bank, 3C11). Antibodies were incubated in PBSTxB overnight at 4°C. Animals were washed six times for 40 minutes with PBSTx, followed by two times in PBSTxB. Secondary antibodies: goat-anti-rabbit HRP IgG antibody (1:1000; Abcam, ab7097) for anti-H3P and anti-caspase3, goat-anti-mouse HRP IgG antibody (1:800; Invitrogen, G-21040) for anti- α -Ac-Tubulin, anti-VC-1, and anti-Synorf1. Secondary antibodies were incubated overnight at 4°C. Animals were washed six times for 40 minutes with PBSTx. Visualization was possible by performing tyramide amplification with FITC 1:1000 in PBSTxI [PBSTx, 0.01M Imidazole, 0.0015% H₂O₂] for 40 minutes, followed by an additional six washes for 40 minutes in PBSTx before mounting. Fluorescent images were taken using a Nikon AZ-100 multizoom microscope with NIS Elements AR 3.2 software. Neoblasts were counted and normalized to the area (mm²) using ImageJ. Caspase-3 was quantified as the mean fluorescence intensity and normalized the area (mm²) using ImageJ.

Quantitative real-time PCR

RNA was extracted from only intact animals (≥ 10 per condition) and converted into cDNA using the Verso cDNA synthesis kit (Thermo Scientific, AB1453A) following manufacturer's protocol as previously described (Ziman et al., 2020). cDNA was stored at -20° C. Quantitative real-time

PCR (qPCR) was run with SYBR green (Applied Biosystems, 4368706) on the StepOne Real-Time PCR System (Applied Biosystems, 4376357). Analyses were performed using the $\Delta\Delta C_t$ method using the TATA box binding protein domain as a reference gene. MWG Eurofins produced primer sequences. Each experiment used triplicates per condition. All gene expression is represented as fold change in comparison to the control group. Heat maps represents geometric means for each data set using a double gradient colormap with a baseline value of 1.0 (white). Adjusted P values were placed into the center of each data set computed from one-way ANOVA's or two-way ANOVA's.

Single-cell sequencing (SCS) data

Smed-TRAF-1/2, and -2A/B gene expression analysis was obtained via the planarian single-cell database hosted by the Sanchez lab in collaboration with the Zeng lab (www.planosphere.stowers.org), which is publically available on planmine 3.0(www.planmine.mpi-cbg.de) (Davies et al., 2017; Zeng et al., 2018; Brandl et al., 2016; Rozanski et al., 2019)

Statistical analysis

All statistics were performed as previously described (Ziman et al., 2020). One-way ANOVA's and Two-way ANOVA's were performed, and all data is represented as the fold change \pm standard error of the mean (SEM). Statistics were computed by pooling biological replicates from technical replicates for analysis. One-way ANOVA's used multiple comparisons to compare computed within each row with compared columns (simple effects within rows) and compared the mean of each cell with the mean of the control for each row. Both One-way ANOVA's and Two-way ANOVA's did not pair data in rows or use matching, and Gaussian distribution was assumed for all data, in addition to a Dunnett's test to correct for multiple comparisons. All

statistical analysis was carried out using Prism7, Graphpad Software Inc.

(<http://www.graphpad.com>).

References

- Brandl, H., Moon, H., Vila-Farré, M., Liu, S.-Y., Henry, I., Rink, J.C., 2016. PlanMine – a mineable resource of planarian biology and biodiversity. *Nucleic Acids Res.* 44, D764–D773.
- Castillo-Lara, S., Abril, J.F., 2018. PlanNET: homology-based predicted interactome for multiple planarian transcriptomes. *Bioinformatics* 34, 1016–1023.
- Davies, E.L., Lei, K., Seidel, C.W., Kroesen, A.E., McKinney, S.A., Guo, L., Robb, S.M., Ross, E.J., Gotting, K., Alvarado, A.S., 2017. Embryonic origin of adult stem cells required for tissue homeostasis and regeneration. *Elife* 6, e21052.
- King, R.S., Newmark, P.A., 2013. In situ hybridization protocol for enhanced detection of gene expression in the planarian *Schmidtea mediterranea*. *BMC Dev. Biol.* 13, 8.
- Oviedo, N.J., Nicolas, C.L., Adams, D.S., Levin, M., 2008. Establishing and maintaining a colony of planarians. *CSH Protoc.* 2008, pdb-prot5053.
- Oviedo, N.J., Nicolas, C.L., Adams, D.S., Levin, M., 2008. Gene knockdown in planarians using RNA interference. *CSH Protoc.* 2008, pdb-prot5054
- Pearson, B.J., Eisenhoffer, G.T., Gurley, K.A., Rink, J.C., Miller, D.E., Sánchez Alvarado, A., 2009. Formaldehyde-based whole-mount in situ hybridization method for planarians. *Dev. Dyn.* 238, 443–450.
- Rouhana, L., Shibata, N., Nishimura, O., Agata, K., 2010. Different requirements for conserved posttranscriptional regulators in planarian regeneration and stem cell maintenance. *Dev. Biol.* 341, 429–443.
- Rozanski, A., Moon, H., Brandl, H., Martín-Durán, J.M., Grohme, M.A., Hüttner, K., Bartscherer, K., Henry, I., Rink, J.C., 2019. PlanMine 3.0—improvements to a mineable resource of flatworm biology and biodiversity. *Nucleic Acids Res.* 47, D812–D820.
- Wurtzel, O., Cote, L.E., Poirier, A., Satija, R., Regev, A., Reddien, P.W., 2015. A generic and cell-type-specific wound response precedes regeneration in planarians. *Dev. Cell* 35, 632–645.
- Zeng, A., Li, H., Guo, L., Gao, X., McKinney, S., Wang, Y., Yu, Z., Park, J., Semerad, C., Ross, E., et al., 2018. Prospectively isolated tetraspanin + neoblasts are adult pluripotent stem cells underlying planaria regeneration. *Cell* 173, 1593–1608.e20.
- Ziman, B., Karabinis, P., Barghouth, P., Oviedo, N.J., 2020. Sirtuin-1 regulates organismal growth by altering feeding behavior and intestinal morphology in planarians. *J. Cell Sci.* 133, 239467.